Ti-Si-C IN-SITU COMPOSITE AS A POTENCIAL MATERIAL FOR LIGHTWEIGHT SOFC INTERCONNECTS

Podhurska[a] V., Brodnikovskyi[b] D., Vasyliv[a] B., Gadzyra[b] M., Tkachenko[c] S., Čelko L., Ostash[a] O., Brodnikovska[b] I., Brodnikovskyi[b] Ye., Vasylyev[b] O.

[a]*Karpenko Physico-Mechanical institute of NASU, Naukova str. 5, 79060, Lviv, Ukraine*
[b]*Frantsevich Institute for Problems of Materials Science of NASU, Krzhizhanivsky str. 3, 03680, Kyiv, Ukraine*
[c]*Central European Institute of Technology, Brno University of Technology, Purkyňova 656/123, 612 00 Brno, Czech Republic*

Due to the investigation of the fracture surfaces of the Ti–Si–Al–Zr samples tested at various temperatures [1, 2], structural and metallurgical aspects of the composite strength change have been observed. This material is similar to the Ti–Si–C material under study. It is known that in the relatively coarse-grained materials of the Ti–Si–Al–Zr system, the transgranular cleavage micromechanism dominates at temperatures up to 500 °C. There are some areas where the crack grew without changing the micro-relief of the fracture surface over a distance of several grains. In these cases, the intermetallic phase $(Ti, Zr)_5Si_3$ did not affect either the fracture character or the fracture toughness level. In this temperature range (20–500 °C), only brittle fracture occurs where the fracture toughness is determined by the presence of defects in the material. With the change in the microstructure of the composites, the micromechanism of crack propagation changes qualitatively. The fine-grained microstructure formed by special thermomechanical treatment [3] causes higher fracture toughness and strength. In such materials, unlike coarse-grained ones, the dislocation mechanism of stress relaxation during crack growth dominates. Fine titanium silicide precipitations and intermetallics located at the (α, β)-titanium boundaries, reducing the effective size of the sliding plane, contribute to the formation of a weakly disoriented cell microstructure. Therefore, dimple fracture of the samples occurs. On fracture surfaces of coarse-grained composite samples tested at temperatures above 500 °C, ductile fracture components appear as a result of

plastic deformation. The Ti_5Si_3 silicide particles failure is brittle. However, these particles are not separated from the titanium matrix even at 900 °C, indicating that there is a high cohesive strength of the matrix-inclusion boundaries. As the material becomes more ductile with increasing test temperature, the microcracking of the intermetallic particles becomes more frequent, reducing thus the effect of structural inhomogeneity of the composites. Such structural changes contribute to the strength of coarse-grained composites at 600 °C, while in the fine-grained materials it is somewhat reduced, which is due to an increase in their ductility.

An increase in the fracture toughness of coarse-grained composites at temperatures above 600 °C was noted. Unlike the behavior of the materials at lower temperatures, where there are still some signs of brittle intergranular cracking, the dimple fracture micromechanism dominates here, and the fracture toughness is obviously proportional to the depth of the dimples and the yield stress. At temperatures above 700 °C, this micromechanism begins to change with high-temperature intergranular fracture, and already in the temperature range of 800–900 °C, the fine-grained composites are inferior to the coarse-grained ones in terms of fracture toughness. Obviously, the high temperature fracture toughness of the composites is proportional to the size of the titanium grains and eutectic colonies and their strength, including the cohesive strength.

1. Experimental

The starting components were a nanosized powder of nonstoichiometric silicon carbide (a solid solution of carbon in silicon carbide, SiC–C) [4, 5] and titanium hydride powder produced from titanium sponge (as per TU U 14-10-026-98) produced by the PJSC "Titanium Institute". The powder of nanosized SiC is characterized by a low lattice parameter (a = 0.43528 nm) and specific surface area of 18–25 m^2/g. Titanium hydride and SiC–C powders were mixed in a planetary-ball mill unit in ceramic drums with hard-alloy balls for 30 min. The powder mixtures were compacted in a steel tool set. The compacts were thermally treated in a vacuum furnace at 1200 °C for 1 h in medium vacuum (as per GOST 5197–85). After that, the compacts were ground in a planetary-ball mill for 30 min to obtain the powder of

composite material of Ti–Si–C system. The Ti–Si–C composite material was sintered of the powder using the industrial installation SPD-120 with induction heating, developed in the special designer bureau at I.M. Frantsevich Institute for Problems in Materials Science of the NAS of Ukraine, in air at 1250 °C and an isostatic pressure of 35 MPa. Temperature control was carried out using an optical pyrometer whose measurement accuracy did not exceed ±20 °C.

The X-ray diffraction (XRD) analysis for determining phase composition of the material investigated was carried out using a X-ray diffractometer SmartLab 3 kW (Rigaku, Japan), while the evaluation of phase composition was carried out by the Rietveld method using HighScore Plus software (PANalytical, The Netherlands).

The metallographical preparation of Ti-Si-C composite samples was done by conventional techniques of wet grinding and diamond paste polishing using the automated preparation system Tegramin 30 (Struers, Denmark). The final mechanical-chemical polishing was carried out using a Struers suspension of OP-Chem.

The microstructure of Ti-Si-C composite was examined using the scanning electron microscope (SEM) Lyra 3 (Tescan, Czech Republic) equipped with the energy-dispersive X-ray spectroscopy (EDS) detector XFlash 5010 (Bruker, USA) both in secondary electron (SE) and back-scattered electron (BSE) imaging modes.

To study mechanical behavior of the material in various modes three-point bend test was performed using beam samples of size 5×5×35 mm [6, 7]. At least 3 samples were used for each test mode. Samples were tested in as-received state in air at 20°C (mode 1), after exposure for 3 h in air at 600°C (mode 2) and for 3 h in hydrogen at 600°C (mode 3). For testing in hydrogen, samples were placed in a sealed chamber, which provided heating using electrical resistance furnace.

The relative stiffness E/E_0, where E is Young's modulus, was estimated by the ratio between tangents of the slopes of linear domains of the corresponding "stress–flexure" diagrams for the material after treatment and in the as-received state.

The specific electrical conductivity σ was determined in air at 20°C by the four-point scheme [8].

2. Results and discussion

The pattern collected from the pristine Ti–Si–C composite sample is shown in Fig. 1. Results of XRD analysis is summarized in Table 1. Four phases were identified in this composite material. According to the XRD results, the TiC, Ti_5Si_3, α-Ti, and Ti_3SiC_2 phases content was found to be 15.1 wt%, 10.8 wt%, 62.3 wt%, and 11.8 wt%, respectively.
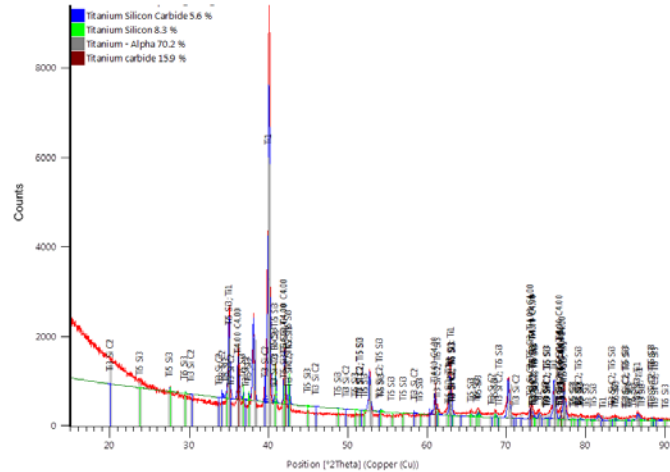

**Fig. 1.** The XRD pattern collected from the pristine Ti–Si–C composite sample.

Table 1. The data of XRD analysis of the pristine Ti–Si–C composite (see Fig. 1)

Phase	Reference code	Compound name	Crystallographic parameters	Phase content (wt%)
Titanium carbide	96-591-0092	Titanium carbide TiC	Crystal system: Cubic Space group: Fm-3m Space group number: 225	15.1
Titanium silicon	98-006-2591	Titanium silicide (5/3) Ti_5Si_3	Crystal system: Hexagonal Space group: $P6_3$/mcm Space group number: 193	10.8
Titanium (alpha)	98-005-2522	Titanium (alpha)	Crystal system: Hexagonal Space group: $P6_3$/mmc Space group number: 194	62.3
Titanium silicon carbide	98-008-8578	Titanium silicon carbide (3/1/2) Ti_3SiC_2	Crystal system: Hexagonal Space group: $P6_3$/mmc Space group number: 194	11.8
Total				100.00

The morphology of these phases was investigated in details using the microstructure images made at various magnifications. At low magnifications, one can see quite homogeneous microstructure of the Ti–Si–C composite (Fig. 2a, b). A small amount of pores of 10–90 µm in size can be detected. The porosity of the composite is about 0.2–0.4%. At higher magnifications, we can observe distinct microstructural components of the Ti–Si–C composite (Fig. 2c, d).
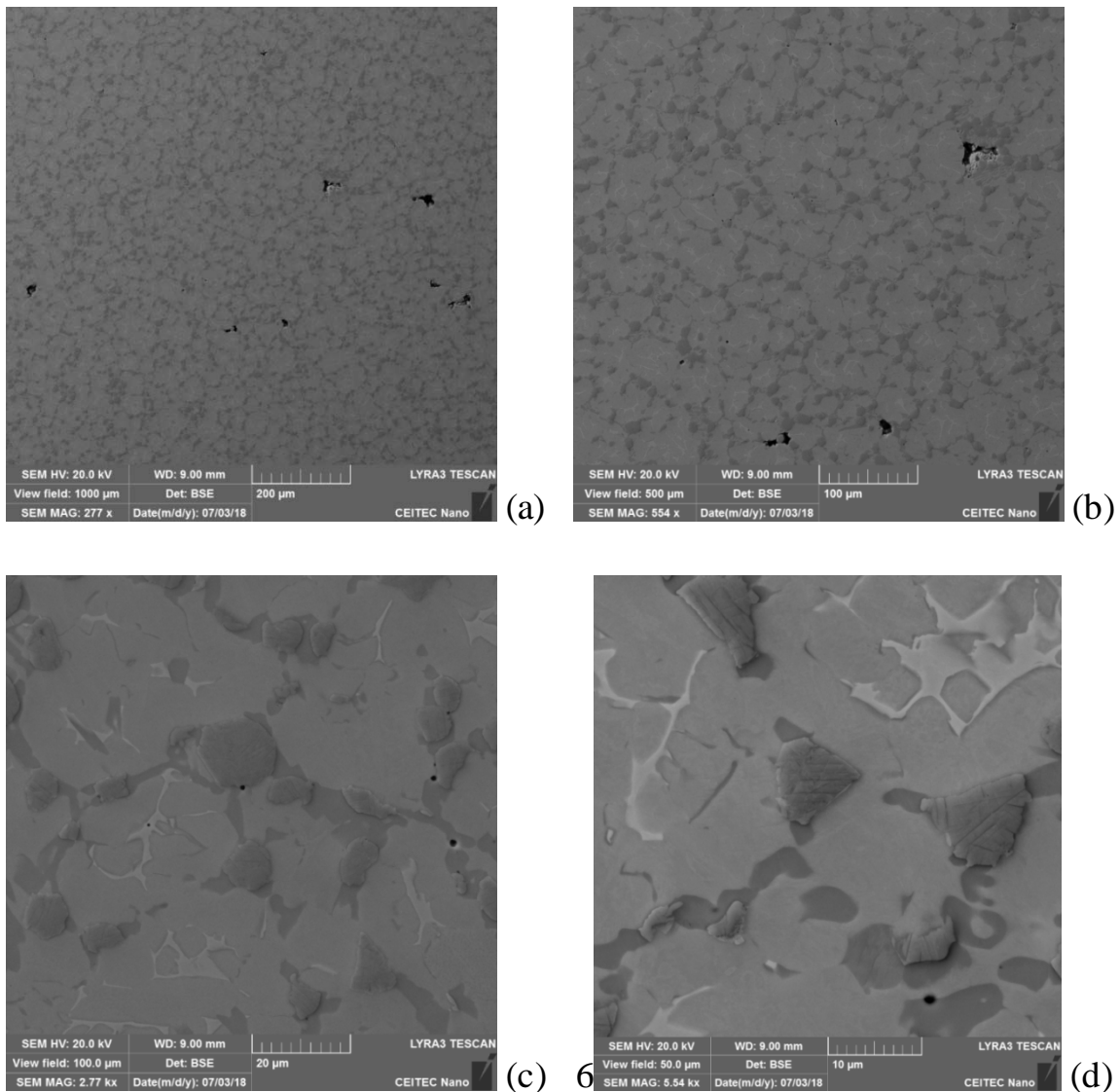
Fig. 2. SEM microstructure of the Ti–Si–C composite in as-received state at various magnifications. Scale bars: 200 µm (a), 100 µm (b), 20 µm (c), and 10 µm (d).
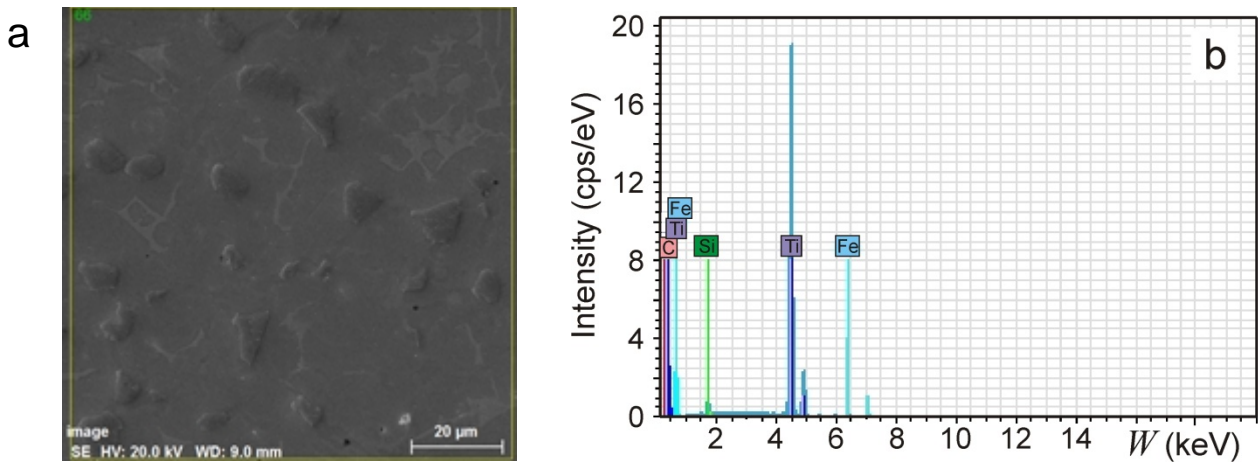
Fig. 3. SEM microstructure (scale bar 20 µm) of the Ti–Si–C composite in as-received state (a) and corresponding spectra of EDS analysis (b).

Table 2. The data of XRD analysis of the pristine Ti–Si–C composite (see Fig. 1)

| Element	wt%	at%
C K	1.21	4.62
Si K	1.39	2.27
Ti K	96.54	92.41
Fe K	0.86	0.70
Total	100.00	100.00

The results of EDS analysis showed some difference in chemical composition of the Ti–Si–C composite material as compared to the results of XRD analysis. According to EDS analysis (Fig. 4 and Table 3), this material is a metal-matrix composite of Ti–Si–C system with high titanium content (about 65–67 vol%). It possibly comprises the titanium carbide phase, MAX-phase, titanium phase with high iron content (intermetallic phase), and titanium matrix phase.

The titanium carbide phase (TiC, see spectra 67–69 in Fig. 4) is in the form of distinct compacted particles of dark-gray color about 10 µm in size. The particles are distributed more or less uniform at the boundaries encompassing a few titanium lamella packets. The total amount of the titanium carbide phase estimated optically using the microstructure image (Fig. 2b) is about 13–15 vol%.

The silicon enriched titanium phase with a small amount of carbon composition looks like drowned areas of dark-gray color about 5 µm in size (see spectra 73–75 in Fig. 4). These areas united sometimes in colonies are located at the boundaries of titanium lamella packets similar to the titanium carbide phase. Maybe, they comprise both the titanium silicide (Ti_5Si_3) and MAX-phase (Ti_3SiC_2) identified by XRD analysis (see Table 1). The total area occupied by them (Fig. 2b) is about 7–10 vol%.

The intermetallic phase consisting of about 89.3 wt% Ti, 0.9 wt% C, 8.4 wt% Fe, 0.76 wt% Cr, and 0.6 wt% Ni (see spectra 70–72 in Fig. 4 and Table 3) is located at the boundaries of separate titanium lamella packets. It is mostly in the form of thin laths of light-gray color but sometimes appears like lath packages. In most cases, this phase does not interfere with the titanium carbide phase or MAX-phase (Fig. 2b). Since the total amount of the intermetallic phase (Fig. 2b) seems to be about 3–5 vol%, it was not identified by XRD analysis (see Table 1).

The titanium phase (α-Ti of about 99 wt% Ti, see Table 3) with a small amount of carbon (about 0.6 wt%) and silicon (about 0.4 wt%) is a matrix phase. Its amount in the composite is about 70–75 vol%.
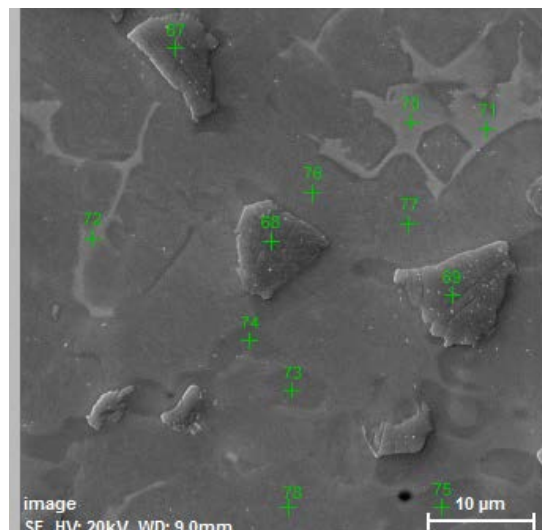
Fig. 4. SEM (SE) image of the Ti–Si–C composite microstructure and the locations of EDS analysis spectra.

Table 3. The data of EDS analysis of chemical composition (in wt%) of Ti–Si–C composite phases (see spectra 67–78 in Fig. 4)

Spectrum	Element						Phase
	C	Si	Ti	Fe	Cr	Ni	
67	5.64	–	94.36	–	–	–	1
68	6.14	–	93.86	–	–	–	
69	5.03	–	94.97	–	–	–	
70	0.97	–	89.44	8.24	0.79	0.56	2
71	0.83	–	89.40	8.36	0.78	0.63	
72	0.85	–	89.10	8.72	0.73	0.60	
73	1.79	21.35	76.86	–	–	–	3
74	1.61	21.17	77.22	–	–	–	
75	1.85	20.63	77.52	–	–	–	
76	0.95	0.64	98.41	–	–	–	4
77	0.66	0.35	98.99	–	–	–	
78	0.57	0.40	99.03	–	–	–	

Based on the obtained data of EDS mapping, we can see the areas of a predominance of each phase presented and locations of the boundaries of formed aggregates consisting of titanium lamella packets (Fig. 5).

Thus, distributed in titanium phase, the colonies of the titanium carbide and silicide phases and MAX-phase encompass aggregates of 50–80 µm in size consisting of a few titanium lamella packets whereas the intermetallic phase is mostly located at the boundaries of the packets inside such aggregates (Figs. 2b and 5). Thus, the subsequence of phases formation may be as follows: in the beginning of sintering process, titanium carbides and silicides and MAX-phase were formed; then, the recrystallization of titanium grains occurred; finally, the intermetallic phase was formed at the boundaries of growing titanium lamella packets.
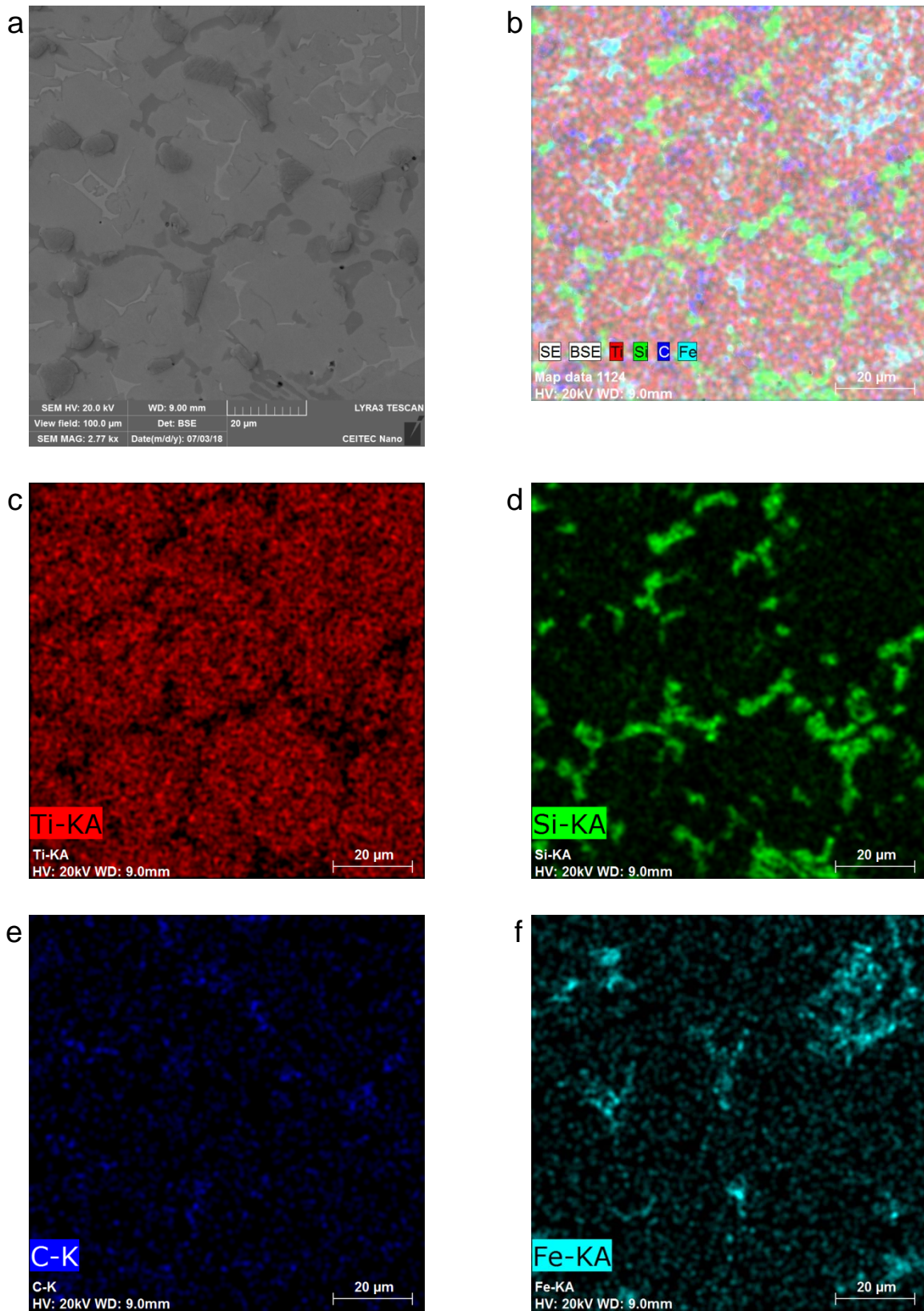
Fig. 5. SEM microstructure (scale bar 20 µm) of the Ti–Si–C composite in as-received state (a) and corresponding EDS maps of distribution of all presented elements (b), Ti (c), Si (d), C (e), and Fe (f).

A positive effect of the operating temperature (600 °C) on its plasticity (30% reduction of the Young's modulus, see Table 4) and strength was revealed for the Ti–Si–C composite (Fig. 6). The ultimate bend strength of the composite at 600 °C is twice as high as at 20 °C (Table 4). This positive effect is further enhanced in hydrogen.

No change in electrical conductivity of the material after testing in hydrogen at 600 °C was detected comparing to as-received state (Table 4), whereas substantial drop of electrical conductivity was found after holding for 3 h and testing samples in air at 600 °C due to thin titanium oxide film formed on their surface.

Table 4. The testing modes for the Ti–Si–C composite and corresponding ultimate bend strength (σ_f), relative stiffness (E/E_0), and electrical conductivity (σ)

Testing mode				σ_f (MPa)	E/E_0 (%)	σ (S/m)
Mode marking	Holding time (h)	Atmosphere	Testing temperature ($\degree C$)			
1	–	air	20	493	100.0	$1.2 \cdot 10^5$
2	3	air	600	939	69.7	$4.4 \cdot 10^3$
3	3	hydrogen	600	1061	70.1	$1.2 \cdot 10^5$
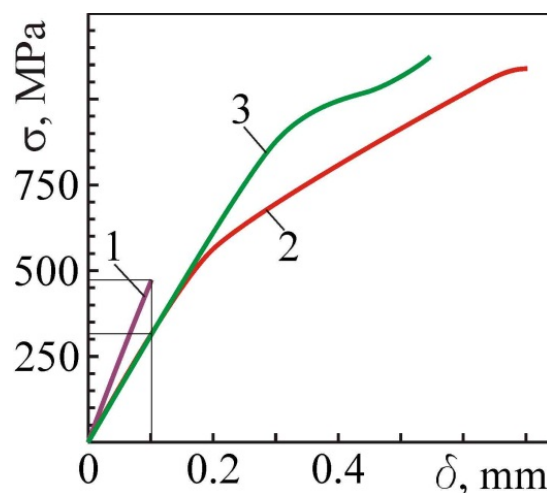
Fig. 6. Stress vs displacement dependences for Ti–Si–C samples tested under three-point bending in as-received state in air at 20°C (mode 1), after exposure for 3 h in air at 600°C (mode 2), and for 3 h in hydrogen at 600°C (mode 3). The numbers near the curves correspond to test modes.

Comparing the composites of Ti–Si–Al–Zr and Ti–Si–C systems, we note the similarity of their microstructures. Based on the results of EDS analysis of the Ti–Si–C composite sample tested under three-point bending in as-received state in air at 20 °C, an increased concentrations of silicon (1.05 wt%) and carbon (3.12 wt%) at the grain boundaries were found (Fig. 7 and Table 5) as compared to their contents in titanium grains (respectively 0.75 wt% and 1.87 wt%). Taking into account general percentage of silicon (4.08 wt%) and carbon (5 wt%) in the bulk of the material (Fig. 7a and Table 5), it was concluded that most of these elements were located at the boundaries of titanium grains as constituents of the the titanium carbide phase and MAX-phase.
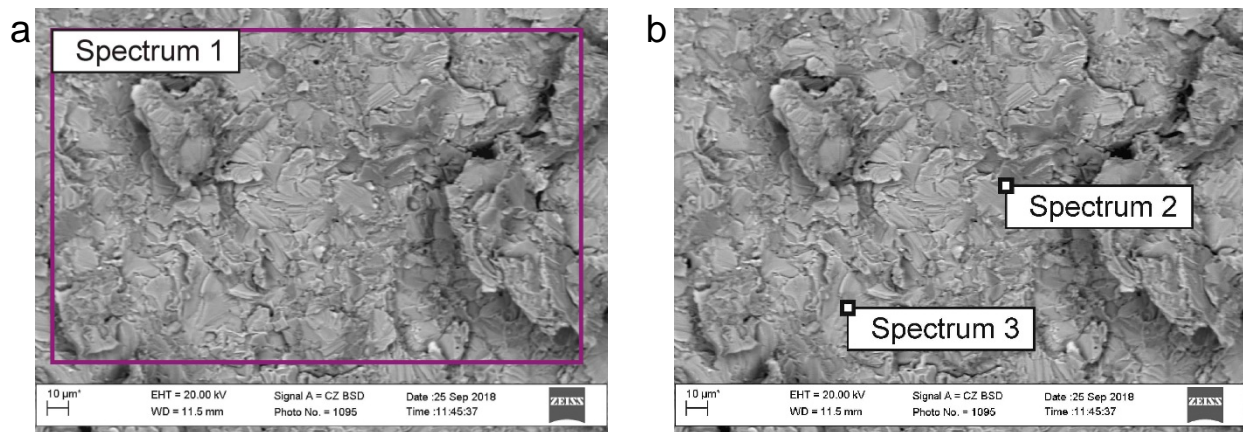

Fig. 7. EDS analysis of the Ti–Si–C sample tested under three-point bending in as-received state in air at 20°C (scale bar 10 µm): (a) spectrum 1; (b) spectra 2 and 3.

Table 5. The data of EDS analysis of the Ti–Si–C sample tested under three-point bending in as-received state in air at 20°C (see spectra 1–3 in Fig. 7)

| Element	Spectrum					
	1		2		3	
	wt%	at%	wt%	at%	wt%	at%
C K	5.00	16.92	3.12	11.31	1.87	7.03
Si K	4.08	5.91	1.05	1.62	0.75	1.21
Ti K	90.92	77.17	95.83	87.07	97.38	91.76
Total	100.00	100.00	100.00	100.00	100.00	100.00

Therefore, in the Ti–Si–C composite under study at 20 °C in air, fracture is initiated by microcracking of the brittle titanium carbide and silicide phases and MAX-phase at the boundaries of the α-titanium lamella packets and consists in brittle cleavage through the titanium grains (Fig. 8a, b). Due to the increase in plasticity of the titanium matrix at 600 °C, brittle fracture of the titanium carbide and silicide phase inclusions and MAX-phase at 600 °C does not lead to the transgranular propagation of the microcracks generated at the grain boundaries of the α-titanium lamella packets.
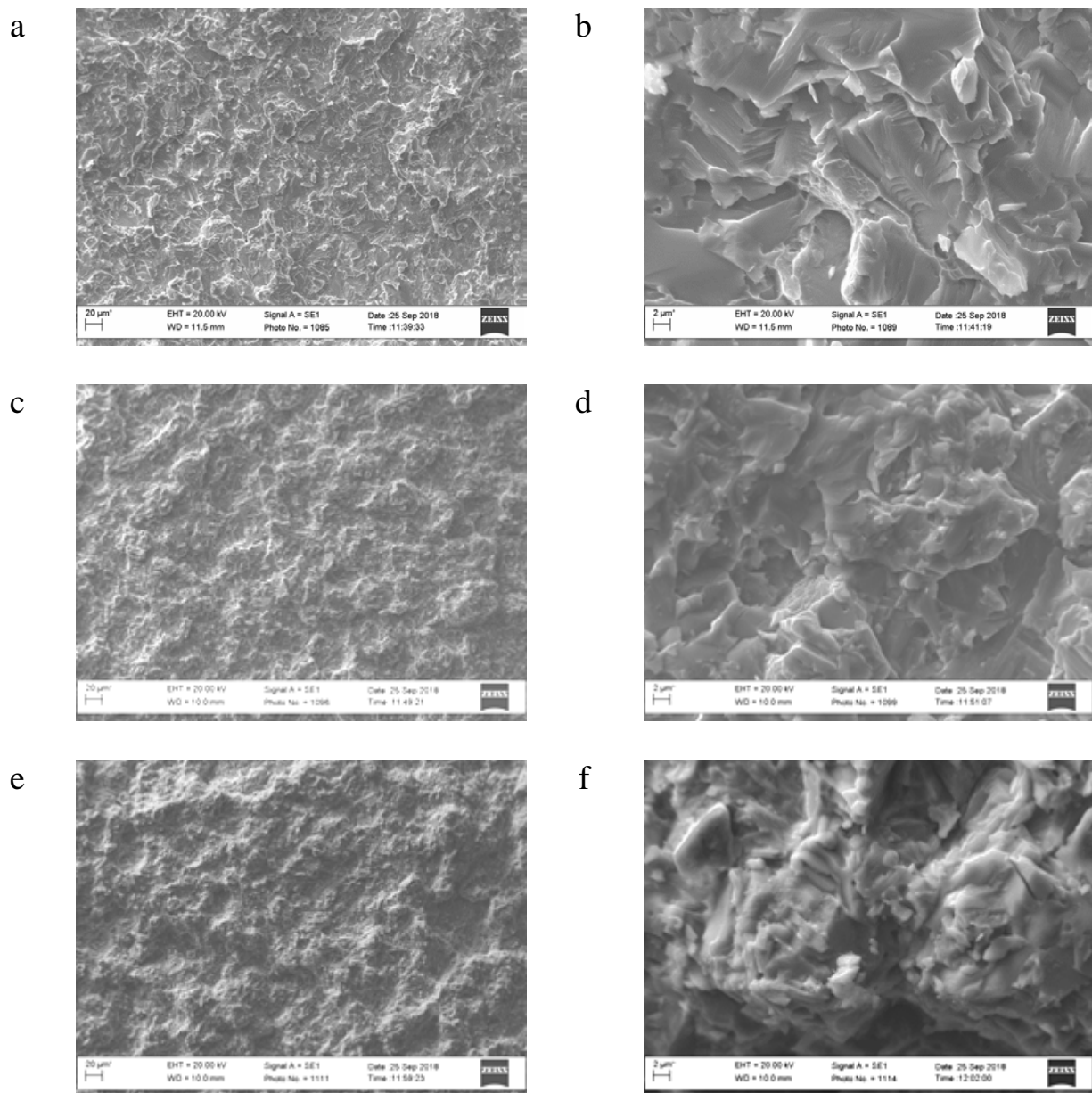
Fig. 8. SEM fractography of Ti–Si–C samples tested under three-point bending in as-received state in air at 20°C (a, b), after exposure for 3 h in air at 600°C (c, d), and for 3 h in hydrogen at 600°C (e, f). Scale bars: 20 µm (a, c, e) and 2 µm (b, d, f).

Therefore, at this temperature, the composite does not fracture even under the stress causing significant plastic deformation of α-titanium grains [1, 2, 9, 10]. Under these conditions, the size of the local stress zone in the vicinity of the main crack tip and stress magnitude increase. This is reflected in the high-energy dimple fracture micromechanism (Fig. 8c, d). At this temperature, the yield strength of the material increases in hydrogen due to the partial embrittlement of titanium grains (Fig. 6), which is reflected in the even more distinctive dimple fracture micromechanism (Fig. 8e, f) [9–11].

At higher magnifications (Fig. 9), we can see the signs of transverse fracture of titanium lamella packets in hydrogen at at 600 °C. Neither the titanium carbide nor titanium silicide nor MAX-phase serves for nucleating microcracks at the boundaries of titanium lamella packets because of increased plasticity of titanium. On the other hand, because of hydrogen assisted partial embrittlement of the titanium matrix phase, the cleavage stress of titanium lamella possibly increases at these conditions reaching the level of yield stress (Table 4 and Fig. 6, see also [12, 13]). This causes predominance of the energy consuming translamellar fracture micromechanism (Fig. 9) and, as a result, an increase in the composite strength (Fig. 6).
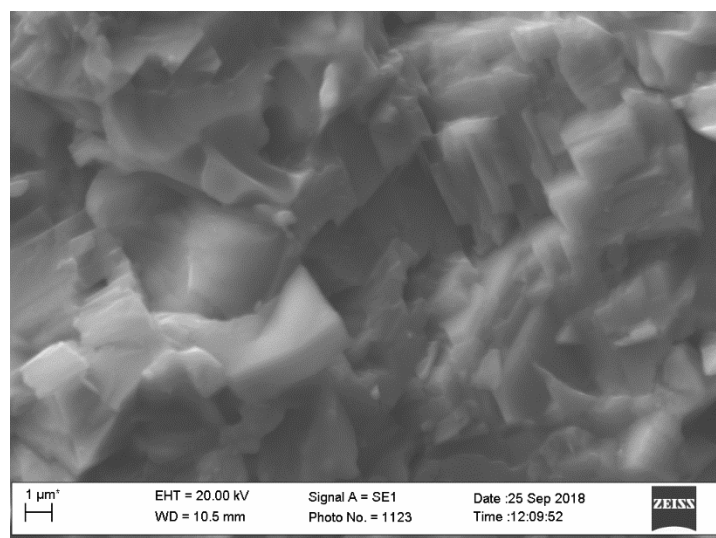
Fig. 9. SEM fractography of Ti–Si–C sample tested under three-point bending after exposure for 3 h in hydrogen at 600°C (scale bar 1 μm).

3. Conclusion

It was found that the bend strength of Ti–Si–C in-situ composite after exposure for 3 h in hydrogen at 600 °C increased substantially as compared to as-received state, due to the change of fracture micromechanism from brittle transgranular clevage of titanium matrix to transverse fracture of titanium lamella packets, along with an increase in material plasticity. The mean values of strength of the material in the initial state and after exposure in hydrogen were 493 MPa and 1061 MPa respectively.

Comparing to as-received state, the specific electrical conductivity of the material after holding for 3 h and testing samples in hydrogen at 600 °C remained the same ($1.2 \cdot 10^5$ S/m). In contrast to this, substantial drop of electrical conductivity (down to $4.4 \cdot 10^3$ S/m) was found after holding for 3 h and testing samples in air at 600 °C, due to thin titanium oxide film formed on the sample surface.

Thus, Ti in-situ composites are quite promising for the application in SOFC power systems and require further investigation.

References

[1] B.D. Vasyliv, Structural optimization of ceramic materials based on crack growth resistance parameters, PhD Thesis, Karpenko Physico-Mechanical Institute, Lviv, 1998 (in Ukrainian).

[2] V.I. Mazur, Yu.N. Taran, S.V. Kapustnikova, V.I. Trefilov, S.A. Firstov, L.D. Kulak, Titanium matrix composites, US Patent 5,366,570 A, 22 Nov 1994.

[3] S.A. Firstov, Structural basis of the strength of refractory metals with a bcc lattice, DSc Thesis, Institute for Problems in Materials Science, Kyiv, Ukraine, 1977 (in Russian).

[4] M.P. Gadzyra, G.G. Gnesin, O.O. Mykhaylyk, Materials Letters, 35 (1998) 277–282.

[5] M.P. Gadzyra, G.G. Gnesin, O.O. Mykhaylyk et al., Diamonds Related Mater. 79 (1998) 1466–1470.

[6] V. Podhurska, B. Vasyliv, in: M.V. Shpotyuk (Ed.), Proceedings of the International Conference on Oxide Materials for Electronic Engineering (OMEE-2012), Publishing House of Lviv Polytechnic, Lviv, 2012, pp. 293–294.

[7] B. Vasyliv, V. Podhurska, O. Ostash, Nanoscale Research Letters, 12:265 (2017).

[8] L.J. Van der Pauw, Philips Research Reports 13 (1958) 1–9.

[9] B. Vasyliv, A. Ivasyshyn, O. Ostash, S. Firstov, V. Mazur, M. Kuzmenko, S. Kapustnikova, in: O.N. Senkov, S.O. Firstov, and D.B. Miracle (Eds.), Metallic Materials with High Structural Efficiency, Kluwer Academic Publishers, Dordrecht, 2004, pp. 235–240.

[10] O.P. Ostash, A.D. Ivasyshyn, B.D. Vasyliv, I.Yu. Okun', Materials Science, 42 (2006) 330–343.

[11] O.P. Ostash, B.D. Vasyliv, A.D. Ivasyshyn, V.Ya. Podhurska, in: V.D. Pokhodenko, V.V. Skorokhod, and Yu.M. Solonin (Eds.), Fundamental Problems of Hydrogen Energetics, KIM Publishing, Kyiv, 2010, pp. 447–467 (in Ukrainian).

[12] D.N. Williams, Hydrogen in Titanium and Titanium Alloys, TML Report No. 100, Titanium Metallurgical Laboratory, Ohio, 1958.

[13] M.J. Donachie Jr., Titanium: A Technical Guide, second ed., ASM International, Ohio, 2000.